Abdominal Imaging

Published online: 29 March 2008

Abdom Imaging (2008) 33:676–688
DOI: 10.1007/s00261-007-9347-5

Staging of colon cancer: whole-body MRI vs. whole-body PET-CT—initial clinical experience

Ettore Squillaci,[1,2] Guglielmo Manenti,[1] Stefano Mancino,[1] Carmelo Cicciò,[1] Ferdinando Calabria,[1] Roberta Danieli,[1] Orazio Schillaci,[1] Giovanni Simonetti[1]

[1]Department of Diagnostic and Molecular Imaging, Interventional Radiology and Radiotherapy, University Policlinic Tor Vergata, University of Rome, "Tor Vergata" Viale Oxford, 81, Rome, Italy
[2]Department of Radiology, University of Rome, "Tor Vergata" Viale Oxford, 81, Rome 00133, Italy

Abstract

Background: To assess the accuracy of whole-body MR imaging (WB-MRI) in comparison with whole-body [18^F]-2-fluoro-2-deoxy-d-glucose (FDG) PET-CT in staging patients with diagnosed colorectal carcinoma (CRC).
Methods: Twenty consecutive patients with previously diagnosed CRC underwent WB-MRI (3T) and PET-CT for staging of lymph node (N) and distant metastases (M). Evaluation was done according to the American Joint Committee on Cancer Staging Criteria. MR images were evaluated by two radiologists while PET-CT images by one radiologist and one nuclear medicine physician. Histology and/or a clinical follow-up of 3–6 months served as standard of reference.
Results: Lymph node involvement was determined in 10/20 cases as N-positive in WB-MRI and in 15/20 in PET-CT. M-stage was evaluated for liver metastases (27 lesions in 15 patients with WB-MRI, 23/15 patients with PET-CT), lung (19/5 patients with WB-MRI, 25/7 patients with PET-CT), and bone (9/3 patients with WB-MRI, 9/3 patients with PET-CT). Two patients showed peritoneal implants and three patients demonstrated local recurrence at the surgery site on both modalities. No brain metastases were found.
Conclusions: WB-MRI is a feasible method for examining colon cancer patients but cannot displace the present role of PET-CT.

Key words: Colorectal carcinoma (CRC)—Whole-body MRI (WB-MRI)—Positron emission tomography (PET) computed tomography (CT)—Colorectal carcinoma staging—Colorectal carcinoma metastasis

Correspondence to: Ettore Squillaci; *email:* ettoresquillaci@tiscali.it

Colorectal carcinoma (CRC) still accounts for approximately 10% of all cancer deaths (79,130 new cases every year and 26,000 deaths resulting annually in US) remaining as the second most common cause of cancer death [1].

Clinical outcome of cancer patients depends crucially on early tumor detection, appropriate staging in operation of effective therapeutic management and accurate follow-up. These purposes are alternatively achieved with the combination of the latest high-resolution morphologic and innovative functional imaging such as computed tomography (CT), and [^{18}F]-2-fluoro-2-deoxy-d-glucose (^{18}F-FDG) positron emission tomography with CT (PET-CT) [2].

Actually, state of the art in CRC screening and staging usually requires a multimodality diagnostic approach but in recent years the introduction of whole body imaging modalities has been undertaken to modify diagnostic concepts for the management of these patients [3–5].

Magnetic resonance imaging (MRI) is a non-ionizing high-resolution technique with excellent tissue contrast and detailed morphological information that appears promising for tumor-spread evaluation. The most recent high field strength MRI scanner with increased signal-to-noise ratio, spatial and temporal resolution, allowed whole body MRI (WB-MRI) with complete coverage head-to-toe with acceptable scanning times and reliable diagnostic ability. Recent technology innovations permit obtaining WB-MRI data sets with no surface coils needed or patient repositioning [6].

Thus, the clinical impact of WB-MRI reported in previous studies in the assessment of metastatic bone marrow involvement [7] provides promising results in staging of malignant tumors or metastases detection compared with PET-CT considered as the reference standard for the tumor staging [8–10].

Furthermore in patients with CRC, PET-CT is utilized in clinical practice for staging, assessment of cancer relapsed lesions, post-treatment changes, and in the evaluation of patients with increasing tumor markers without a known lesion [11–13].

The purpose of our study was to define the potential role of WB-MRI in staging and follow-up of patients with diagnosed CRC compared to morphological and functional findings obtained with PET-CT.

Methods

Patient population

From February to June 2007, 20 consecutive patients (12 male and 8 female; 47–73 years age range; 56 years mean age) with histopathologically proven CRC, were included in the study. Each patient was staged according to the American Joint Committee on Cancer (AJCC) using histopathology results from the resected specimens to assess pTNM parameters [14].

Patients with stage II ($n = 5$) and stage III ($n = 15$) were included in our study as obtained from the original post-surgery pathology reports.

Patients were referred to our protocol for clinical restaging (from 9 months to 3 years after surgery) by evidence of abnormal increase of specific serum tumor markers and/or other imaging findings suspicious for loco-regional recurrence or distant metastases. PET-CT examination chosen as standard of reference demonstrated malignancy progression of previous post-surgery stage assessing all patients as stage IV according to cTNM parameters (AJCC) [14].

WB-MRI exam was performed within 10 days after PET-CT exam. Informed consent was obtained from each patient. Exclusion criteria were based on contraindications to MR imaging, including the presence of a pacemaker, metallic implants in critical organs, severe claustrophobia, and a lack of willingness or ability to sign the informed consent.

PET-CT imaging

All examinations were performed using a discovery ST integrated PET-CT system (GE, General Electric, Medical Systems). This system combines a High-Speed Ultra 16-detector row (912 detectors per row) CT unit and a PET scanner with 100,80 bismuth germanate (BGO) crystals in 24 rings. Patients were instructed to fast for at least 6 h, because glucose competes with [^{18}F]-FDG for cellular uptake. Serum glucose levels were checked before administering [^{18}F]-FDG, and the radiotracer was only injected if blood glucose levels were normal to avoid the diagnostic potential of PET being reduced by the competitive effect of high blood glucose.

Patients with hyperglycemia were invited to take a short walk to increase muscle activity and lower blood glucose to below 150 mg/dL. A dose of 370 MBq of radiotracer was administered intravenously as a single bolus 45–60 min before the examination. During this phase, adequate hydration was maintained with an intravenous infusion of saline (250–500 mL) to reduce pooling of the tracer in the renal system.

Before each acquisition patients were systematically invited to void the bladder to reduce artifacts due to the presence of radio-urine.

A low-amperage (80 mA) non-enhanced CT scan was then acquired to correct attenuation for the PET study. After non-enhanced CT, the PET study was done with 2D technique in the caudocranial direction from the proximal third of the femur to the skull; six to seven beds were acquired (each bed duration was 4 min). Images were reconstructed using a standard iterative algorithm [ordered subsets expectation maximization (OSEM)], for a mean PET examination time of 24–28 min.

Immediately after the PET study, contrast-enhanced CT was carried out with i.v. administration of non-ionic iodinated contrast material (100–120 mL, 370 mgI/mL, 420 mgI/kg at 3 mL/s), obtaining two successive stacks of scans: the first comprised the upper abdomen with a delay of 30 s from the injection onset; the second extended from the neck to the pelvis with 60–80 s delay. Following these acquisitions, a further stack of scans can be used to characterize equivocal hepatorenal lesions.

Finally, after having the patients lower their arms along the trunk, axial scans of the skull were acquired.

The acquisition technique was 120–140 kV, automatic mA (limit 330–350 mA), thickness 3.750 mm (reconstructed at 1.25 mm), acquisition mode 27.50/1.375:1, gantry rotation time 0.6 s, large FOV, matrix 512 × 512. Average total duration of the PET-CT study was 35 min.

Table 1. Technical parameters of different sequences used for 3T WB-MRI

	T1W FFE	T2W TSE	T2W TSE STIR	THRIVE SPAIR
Field of view FOV/rectangular FOV	470/80	470/80	470/80	490/95
Slice thickness/gap/n. of slices	6 mm/3 mm/24–30	6 mm/3 mm/24–30	6 mm/3 mm/24–30	4 mm/–2 mm/50–60
Matrix/reconstructon	256 × 320	256 × 320	256 × 320	240 × 512
TR repetition time/TE echo time/flip angle	500/2.3/70	2000/80/90	3200/120/60	Shortest/shortest/10
NSA	2	2	2	1
Breath-hold	Yes	Yes	Yes	Yes

Multiplanar PET and CT images were reconstructed by means of a standard iterative system and fused with linked cursors (Xeleris, GE Healthcare, Milwaukee, USA).

Magnetic resonance imaging

MRI was performed with a high-field strength 3.0 T scanner (Philips Intera Achieva, Best, Netherlands), with maximum gradient strength and slew-rate set to 80 mT/m and 200 mT/m/ms, respectively, using the quadrature-body (Q-body) coil for radiofrequency (RF) signal emission and reception with a dedicated rolling table patient support.

Patients were examined in the supine feet-head position, covering the entire body as a matrix in combination with automated table movement, with a maximal longitudinal field of view (FOV) of 200 cm.

Whole body images were obtained in the coronal plane with multiple stacks acquisitions (seven or eight overlapped stacks depending on body height) from head-to-toe: head/neck, thorax, abdomen, pelvis, thighs, knees

Table 2. Comparison lesion by lesion of different metastases detected with PET-CT and WB-MRI

		PET-CT	WB-MRI
N	Ilar/mediastinic/axillary/ Abdominal lymph nodes	15	10
M	Brain	0	0
	Lung	25	19
	Liver	23	27
	Bone	9	9
	Other	5	5

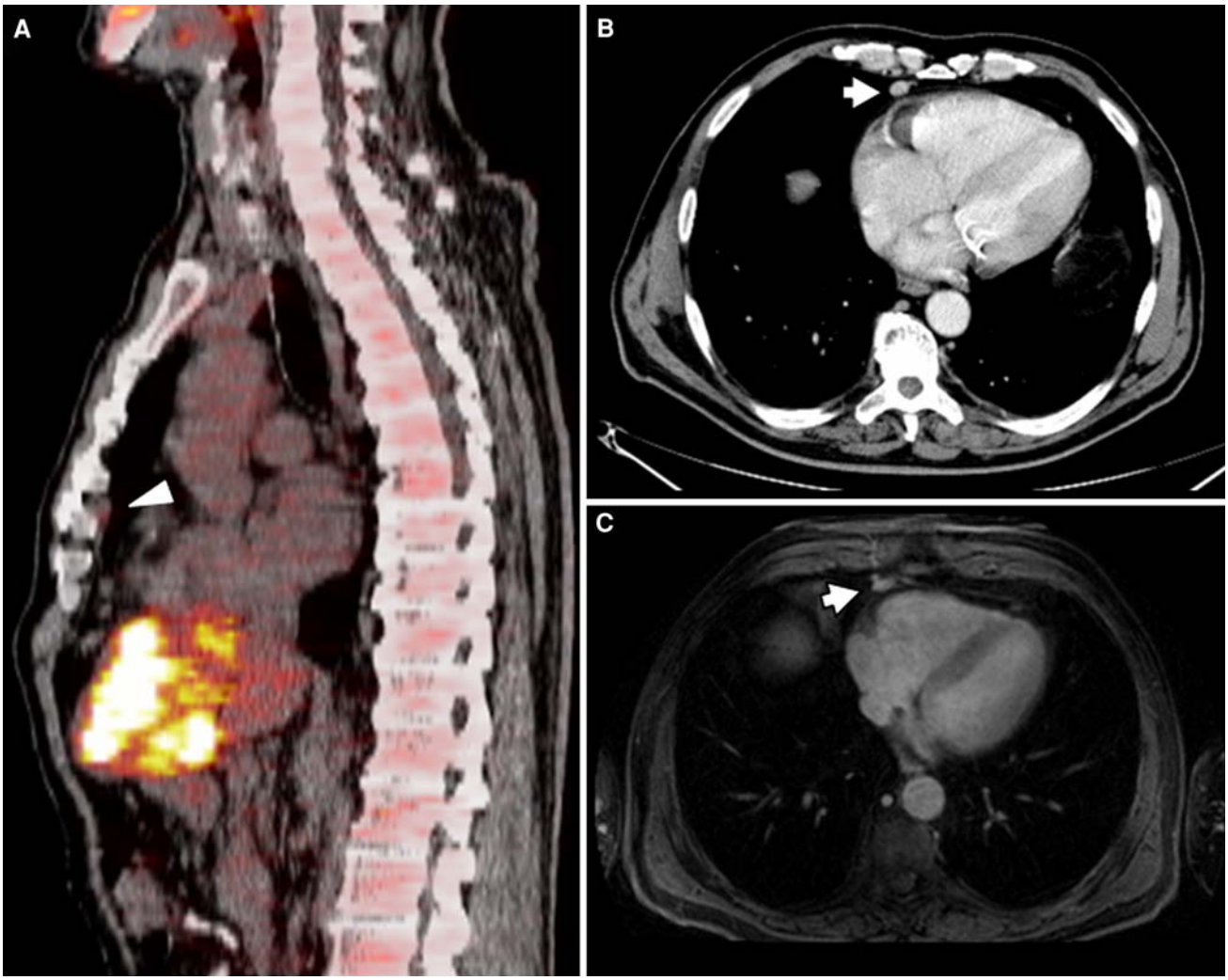

Fig. 1. Sixty-one years-old patient with anterior mediastinic adenopathy. Sagittal PET-CT fused image (**A**), post-contrast axial CT image (**B**) and T1W 3D FFE post-contrast axial image WB-MRI (**C**) at the same level. A 8 mm lymph node with low metabolic activity (*arrowhead*) is visible on PET-CT image. A significant enhancement is visible on both CT and WB-MRI (*arrows*).

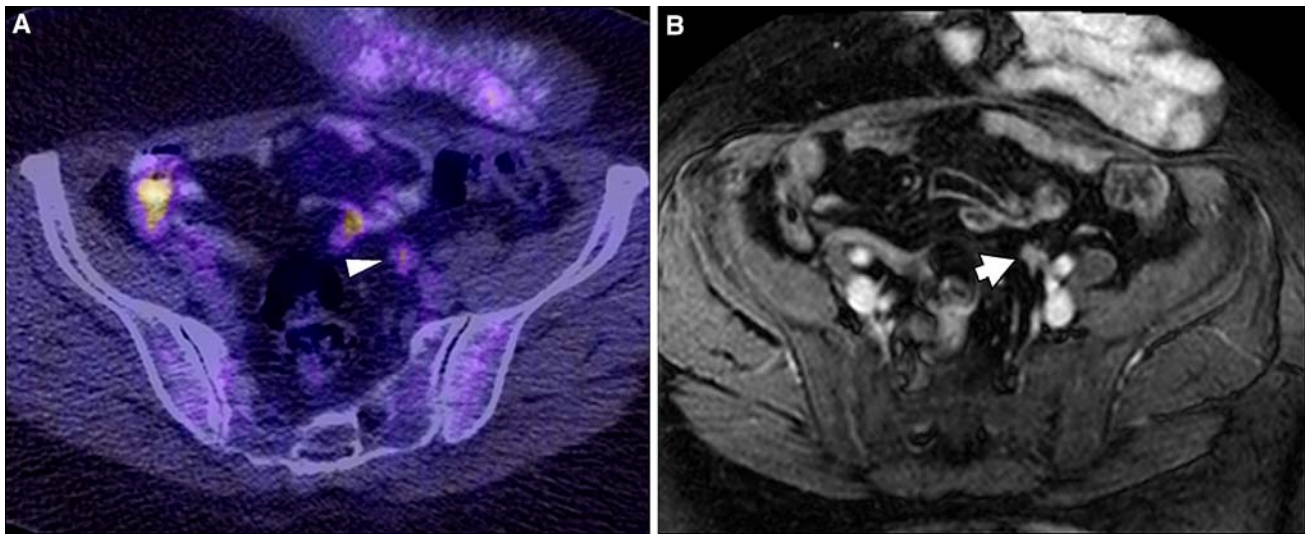

Fig. 2. Fifty-eight years-old patient who underwent left emicolectomy and ileostomy. Transverse PET-CT fused image (**A**) and T1W 3D FFE (THRIVE) post-contrast WB-MRI axial image (**B**). Left-common iliac 15 mm adenopathy with high metabolic activity is well demonstrated on PET-CT (*arrowhead*) with perfect correlation with WB-MRI (*arrow*).

and calves with free-breath technique and breath-hold technique for the thorax, abdomen, and pelvis.

Morphological imaging was obtained with 30/40 slices (depending on body build), with T1 weighted FFE unenhanced sequences, T2 weighted TSE and T2 weighted STIR TSE; multiphasic 3D FFE T1W high-resolution isotropic volume examination sequences with fat suppression (THRIVE) were obtained in the axial plane before and after paramagnetic contrast media (0.2 mmol/kg gadopentetate dimeglumine, Magnevist; Schering, Berlin, Germany) injection (3 mL/s flow rate followed by 20 mL saline solution) at the thorax, abdomen and pelvis levels (Table 1). Finally T1 weighted FFE post-contrast images were obtained with the same parameters in coronal plane from the head-to-toe. Total scan duration for each examination was 47–55 min.

Imaging analysis

The PET-CT data set were evaluated in consensus by a board-certified radiologist and a nuclear medicine specialist on a dedicated workstation (Advantage-Windows 4.2, GE, General Electric, Medical System) after reconstruction with fusion PET-CT software; WB-MRI images data were analyzed in consensus by two board-certified radiologists.

Both reader groups were blinded to other imaging modality findings detected on previous or current diagnostic imaging examinations.

Assessment of lymph nodes and distant metastases or local recurrence in PET-CT images was based on qualitative and quantitative criteria, respectively, according to the evidence of regions of focally increased glucose metabolism uptake and maximal standardized value (SUV). An increased glucose uptake area over surrounding tissue was significant for malignancy.

The assessment of pathologic findings on MR images was determined only for metastatic localization, lymph node involvement (lesion cut-off size of 10–15 mm) or the presence of local recurrence accounting for morphologic features, size, signal intensity changes, and enhancement on dynamic sequences.

Finally, evaluation of malignancy spread was determined individually for both modalities according to (AJCC) TNM staging classification.

The two imaging modalities were compared for the accurate assessment of disease spread but based on the small number of patients included in this feasibility study, no assessment of sensitivity and specificity was performed.

The two imaging modalities were compared for the accurate assessment of disease spread (N- and M-stage) on the basis of a lesion-by-lesion overall analysis (Table 2).

Lesion size detection accuracy was determined for each lesion comparing the results of both imaging modalities.

Standard of reference

The morphological and functional results obtained by PET-CT analysis were considered as the reference standard for the correct assessment of malignancy presence in the definitive interpretation of WB-MRI and relative diagnostic value.

Clinical, histological, and radiological information, obtained within a period of 3–6 months from the beginning of our study, were consulted as a reference method with the PET-CT and WB-MRI data, collected

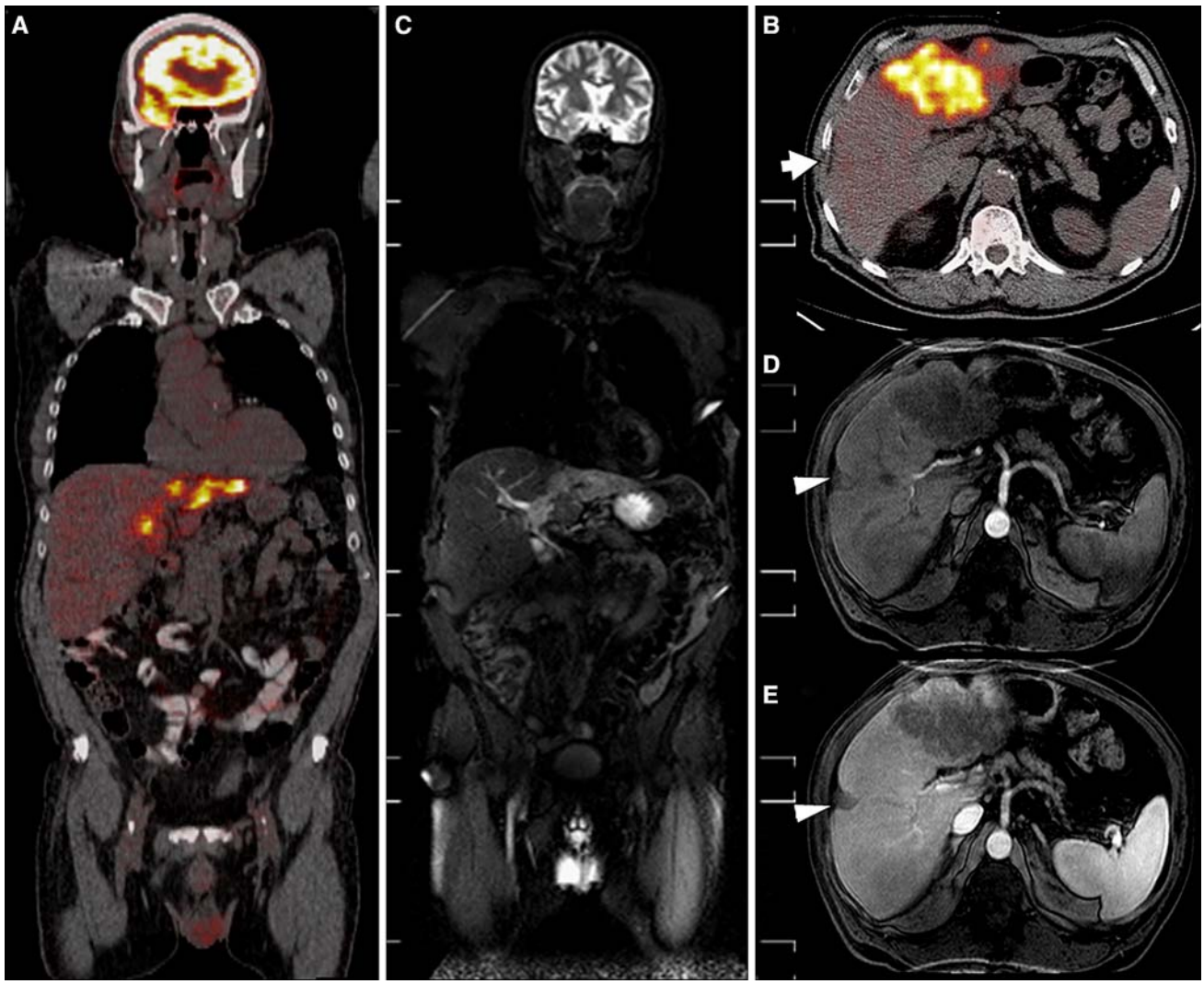

Fig. 3. Sixty-four years-old patient with colorectal carcinoma who underwent thermoablation for hepatic metastasis at the time of surgery, 2 years follow-up. Coronal (**A**) and axial (**B**) PET-CT fused images, coronal T2W TSE STIR WB-MRI (**C**), T1W 3D FFE post-contrast axial images (**D**, **E**). A large hepatic metastasis is well visible on left liver on both PET-CT and WB-MRI. PET-CT shows no activity in the site of previous thermoablation (*arrow*) with no contrast enhancement on T1W 3D FFE post-contrast images (*arrowheads*).

during the study to assess the real diagnostic capability of each modality.

In particular, malignancy progression was assessed on the basis of the evidence of quantitative and qualitative changes (number, size, and contrast enhancement behavior) of lesions, signs of progressive or infiltrative-growth of the lesion or typical features of malignant lesion on other MRI, CT or PET-CT follow-up examinations.

Results

All patients were classified by PET-CT examination at stage IV. No patients were overstaged or understaged according to WB-MR examination results.

A total of 35 lymph nodes in the chest ($n = 12$) and in the abdomen ($n = 23$) were detected by both modalities; 15 were defined as positive for malignancy according to PET-CT and 10 were correctly characterized as N-positive on WB-MRI. PET-CT detected malignant lymph nodes of a median size of 14 mm ± 4 mm ($n = 15$; range 7–34 mm); lymph node median size on WB-MRI was 17 mm ± 7 mm ($n = 10$; range 7–34 mm). The smallest lymph node measured 7 mm ($n = 1$) in diameter on WB-MRI. PET-CT was more sensitive for lymph node involvement in all size groups than WB-MRI. Lymph nodes smaller than 1 cm showed low metabolic activity on PET-CT (Fig. 1) while a high activity was visible for a lesion of 1 cm or more (Fig. 2).

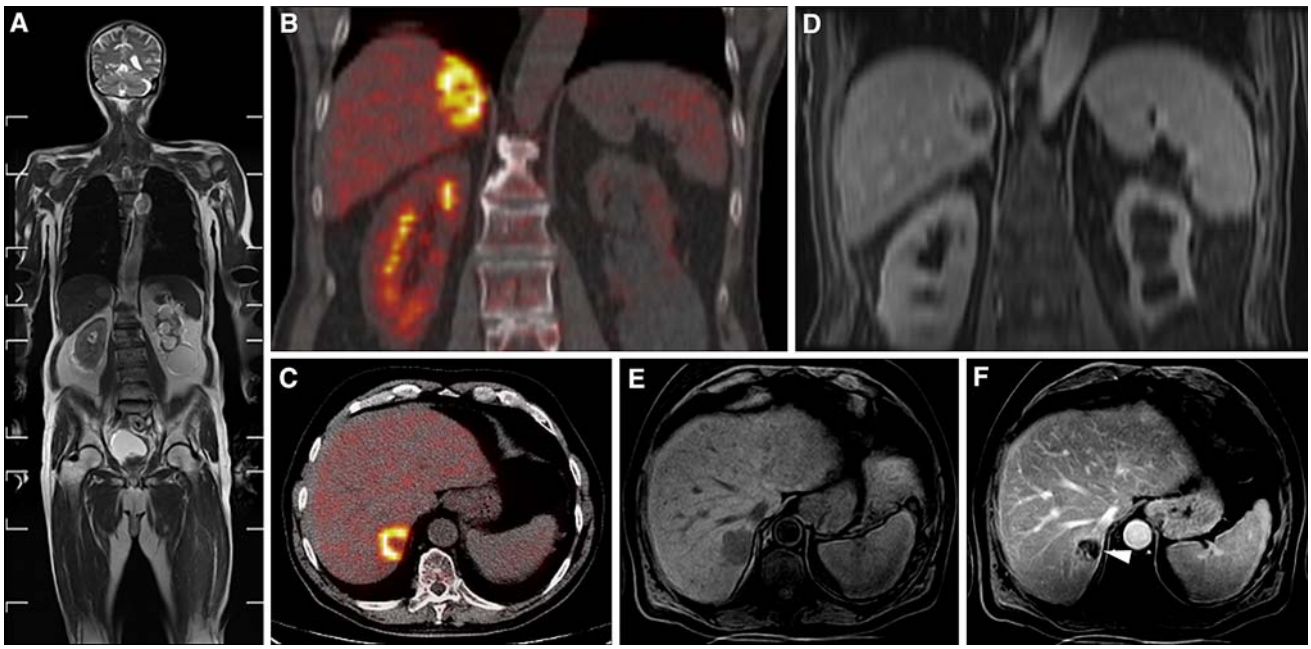

Fig. 4. Sixty-eight years-old patient with right liver metastasis. Coronal T2W TSE WB-MRI (**A**), coronal and axial PET-CT fused images (**B**, **C**) and T1W 3D FFE post-contrast coronal reformation image (**D**) at the same level; T1W 3D FFE pre-contrast (**E**) and post-contrast (**F**) axial images. On PET-CT axial image (**C**) is well defined the peripheral uptake of the lesion properly correlated with the rim-enhancement displayed on T1W FFE post-contrast image (*arrowhead*), demonstrating the necrotic area and the surrounded active portion of the lesion.

WB-MRI detected 27 hepatic metastases in 15 patients (mean size 22 mm ± 4 mm; range 3–42 mm); the smallest hepatic metastasis was 3 mm in diameter (n = 2). PET-CT revealed 23 hepatic metastases in 15 patients identifying a lesion as small as 4 mm (mean size 13 mm ± 4 mm; range 4–38 mm) (Fig. 3). There was always a good correlation between morphologic imaging of WB-MRI and functional imaging of PET-CT regarding evaluation of intralesional necrosis and peripheral activity (Fig. 4). One 8 mm hepatic metastasis, with significance uptake and contrast-enhancement on PET-CT, was not visible on WB-MRI (Fig. 5).

WB-MRI detected 19 pulmonary metastases in five patients (mean size 10 mm ± 3 mm; range 4–30 mm). On WB-MRI the smallest pulmonary metastasis was 4 mm in diameter (n = 2). PET-CT detected 25 lung metastasis in seven patients (mean size of 15 mm ± 5 mm; range 8–30 mm) (Fig. 6). Six metastases measuring 7 ± 3 mm in diameter with no significance to metabolism valuable on PET-CT were visible on WB-MRI (Fig. 7).

Nine bone metastases (spine 6, hip-bone 2, rib 1), demonstrated by increased signal intensity on T2 weighted STIR images (Fig. 8), were detected on WB-MRI in three patients. One spine lesion was missed on PET-CT while a rib lesion was missed on WB-MRI (Fig. 9).

No brain metastases were detected on WB-MRI and PET-CT imaging.

In two patients, a peritoneal metastatic involvement was detected both by PET-CT and WB-MRI (Fig. 10). Recurrence at surgery site was observed in three patients with both modalities (Fig. 11).

Both imaging modalities were performed without adverse effects in all patients.

Discussion

In CRC prognosis, therapeutic options strictly depend on accurate evaluation of tumor extension and early identification of local recurrence and distant metastases. Actually, staging is based on multimodality strategies resulting in a time-consuming and expensive diagnostic approach [2].

Since early 2000s, hybrid scanners such as PET-CT [8–10], were considered the standard imaging reference for cancer staging with high accuracy in detecting both primary tumor and metastatic disease [10–13, 15]. Regard to CRC, PET-CT is the imaging modality with highest sensitivity in detection of primary tumor and liver metastases but it shows a low sensitivity with high specificity in characterization of lymph node involvement. In one study, PET-CT has shown 95% sensitivity in detection of primary site, 78% in evaluation of liver metastases, and 29% in location of lymph nodes metastases [8].

Uptake in the gastrointestinal tract can be variable because of peristalsis; frequently uptake by the cecum

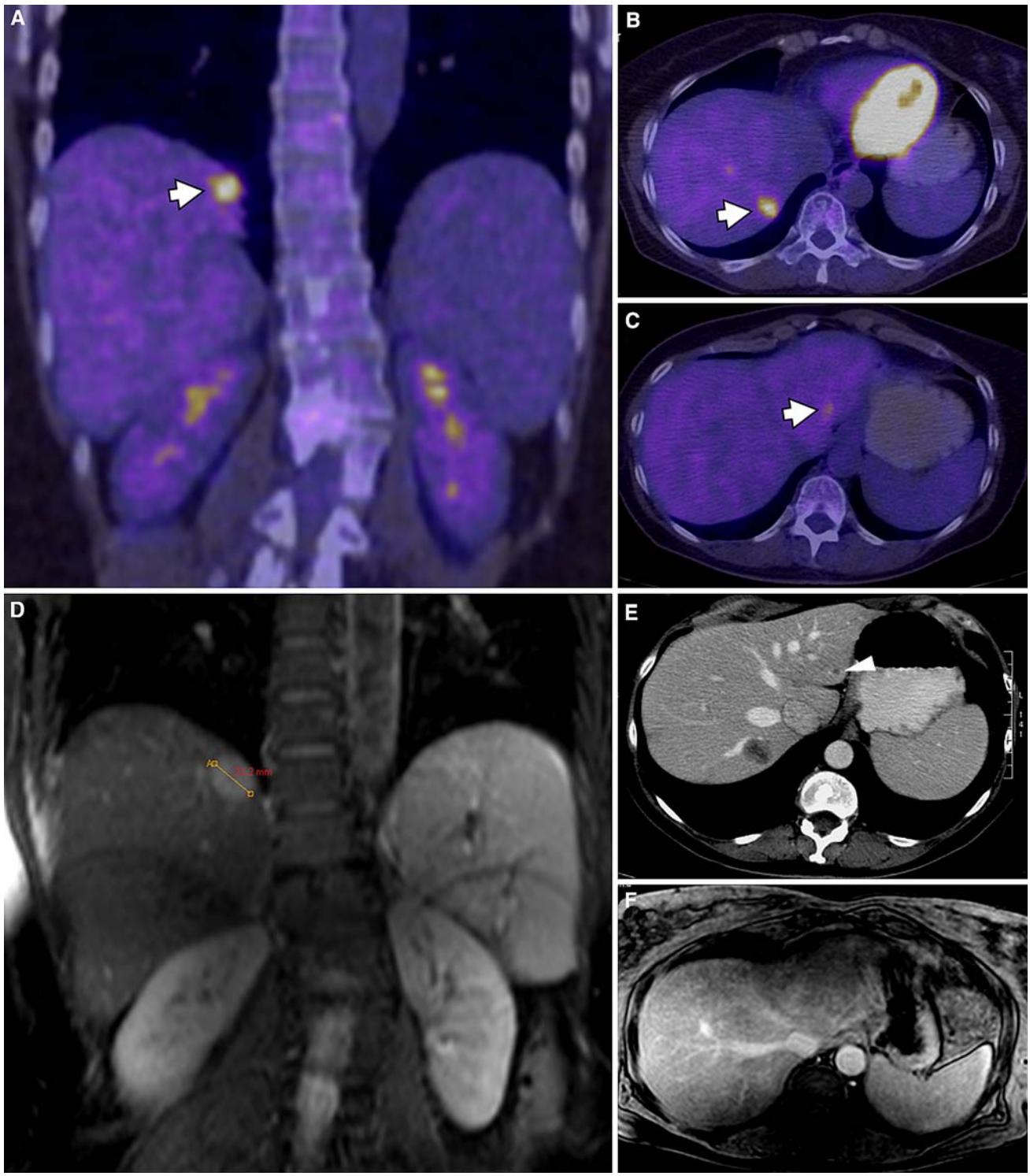

Fig. 5. Sixty-three years-old patient with hepatic metastases 3 years after surgery. Coronal (**A**) and axial (**B**, **C**) PET-CT fused images, post-contrast axial CT image (**E**), T1W FFE post-contrast WB-MRI coronal (**D**) and axial T1W 3D FFE post-contrast image (**F**). Two hepatic metastases are well visible (*arrows*) on PET-CT images (**A**–**C**). There is a tight correlation PET-CT/WB-MRI on coronal images for the larger hepatic lesion while the smaller 6 mm lesion is well evident on post-contrast CT image (**E**, *arrowhead*) and fused PET-CT image (**C**) but is not visible on axial T1W 3D FFE post-contrast image, probably due to respiratory motion artifacts.

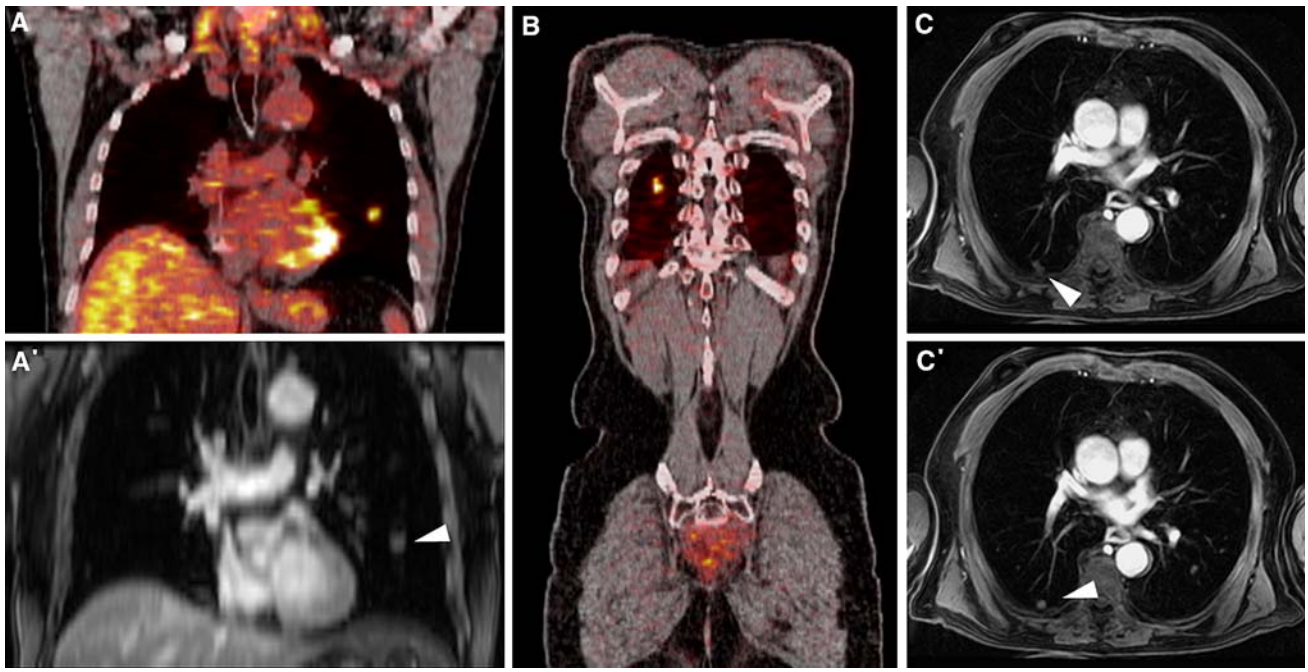

Fig. 6. Seventy-one years-old patient with bilateral lung metastases 2 years after surgery. Coronal PET-CT fused images (**A**, **B**), T1W 3D FFE coronal reformations (**A′**) and axial (**C**, **C′**) images. Lung metastatic lesions (*arrowheads*) ranging 10–17 mm are visible on both WB-MRI and PET-CT.

can be noticeable in absence of lesions because of the presence of lymphoid tissue. False negative findings can be demonstrated in tumors with hypocellularity (like mucinous adenocarcinoma) [9].

The use of WB-MRI in clinical practice for tumor staging has been limited up to now by the long examination time and low quality images due to low spatial and contrast resolution [16].

Recent WB-MRI protocols are based on real-time ultrafast acquisition sequences, allowed by faster magnetic resonance gradient technology and contemporary examination of multiple body areas using rolling table platform [16–19].

Usually WB-MRI is performed using parallel imaging technique (SENSE, SENSitivity Encoding) in order to reduce scan time without compromising temporal and spatial resolution of images [20]. This technique requires the use of multiple surface coils that may induce a claustrophobic effect. However, thanks to the high field strength of today's MR scanners at 3 T, we have obtained comparable results by using a quadrature body coil that permits a reduction in scan time and a better patient compliance. These improvements have allowed the use of WB-MRI in the detection of metastatic bone lesions, in management of neoplastic patients in tumor staging and in evaluation of metastatic disease in compare to PET-CT exam [5, 21–25].

Currently, only few a studies have evaluated the role of WB-MRI in screening of metastases or complete tumor staging, and none in staging of colorectal carcinoma (CRC). Therefore, previous studies are limited in providing final results concerning the overall performance of WB-MRI in tumor staging. Although Schmidt et al. [5] have not found a relevant difference between MRI (91%) and PET-CT (96%), Antoch et al. [22] have shown higher accuracy (77%) of PET-CT compared to 54% for WB-MRI. However, these studies are difficult to compare for differences in techniques, heterogeneity of included tumor types with only a few cases of gastrointestinal cancer in the investigation by Antoch et al. [22].

In this study we tried to investigate the potential role of WB-MRI in staging CRC patients comparing our results with gold standard PET-CT. According to other studies [11, 22], we observed a high-resolution with a low specificity in lymph node involvement assessment, compared to the metabolic information provided by PET-CT.

Functional information provided by PET-CT [22] decreases doubts in case of enlargements due to inflammations or micrometastases localization, allowing both identification and characterization of equivocal nodes. A recent application of WB-MRI in detection of metastatic lymph node disease is based on STIR-EPI-diffusion sequences. This sequence provides, with adequate fat suppression, WB-MRI-diffusion-PET-graphy with high-resolution images of pathological lymph nodes. However, the clinical impact of this application is far from a definitive conclusion [26, 27].

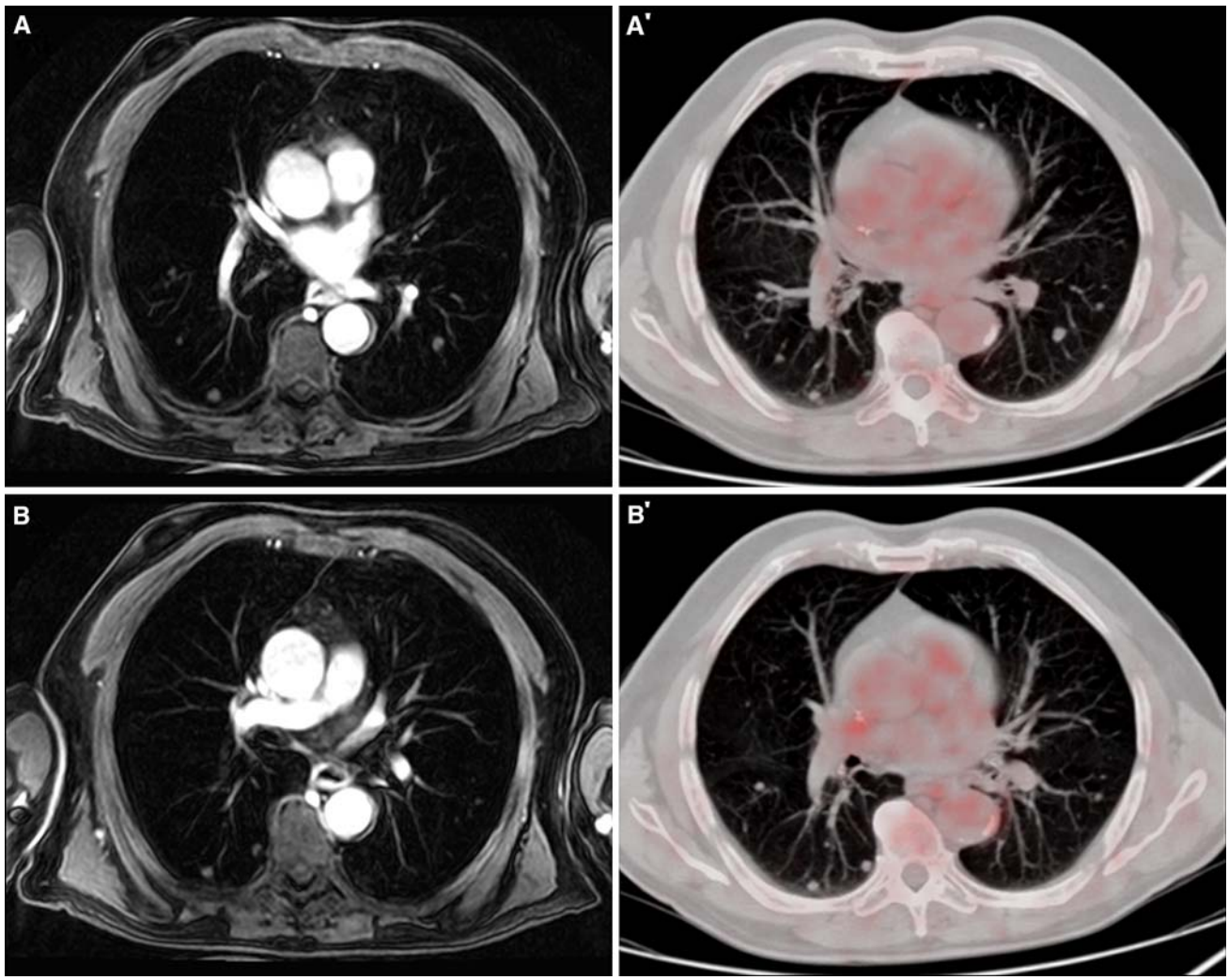

Fig. 7. Fifty-nine years-old patient with multiple lung metastases 4 years after surgery. Axial T1W 3D FFE axial post-contrast images (**A**, **B**) and corresponding axial PET-CT fused images (**A′**, **B′**). Small size lung metastases, ranging 4–8 mm, detectable on MR images do not demonstrate activity on corresponding fused PET-CT images.

There is a trend of superiority for WB-MRI in detecting metastasis in liver [21], brain, and bone [7, 27]. In particular liver studies with dynamic post-contrast sequences (THRIVE), added to multi-stacks acquisition, allow multiphasic and high-resolution evaluation of metastatic lesions without a significant increase of examination time. In the literature, there is no clear agreement about the potential of WB-MRI in metastatic liver localizations compared to PET-CT, although Semelka et al. revealed less accuracy of CT or PET alone than MRI; furthermore, it is still not definitive if the integration of PET and CT helps to reduce this limitation [28, 29]. Rappeport et al., using superparamagnetic iron oxide (SPIO)-enhanced MR imaging, reported greater sensitivity with similar accuracy in metastatic liver assessment between MRI and PET-CT imaging [30–32].

WB-MRI is a reliable technique in evaluations of metastatic bone disease with detailed anatomical information on axial and appendicular skeleton. [6, 7, 16, 33].

Due to the larger field of view of WB-MRI, it is possible to assess more metastatic lesions located outside the diagnostic range of PET-CT. WB-MRI seems to have limitations in detecting metastases of curved flat bones, especially in ribs where additional motion artifacts of respiration and pulsation impair image quality.

Furthermore, WB-MRI is highly effective in the detection of cerebral metastatic disease, crucial for prognosis and therapy. Cerebral and skull metastases are particularly difficult to identify in PET-CT because of a high physiological tracer uptake in normal brain tissue.

The many advantages of high sensitivity, specificity, and accuracy of PET-CT [8, 10, 11, 13, 22] coexist

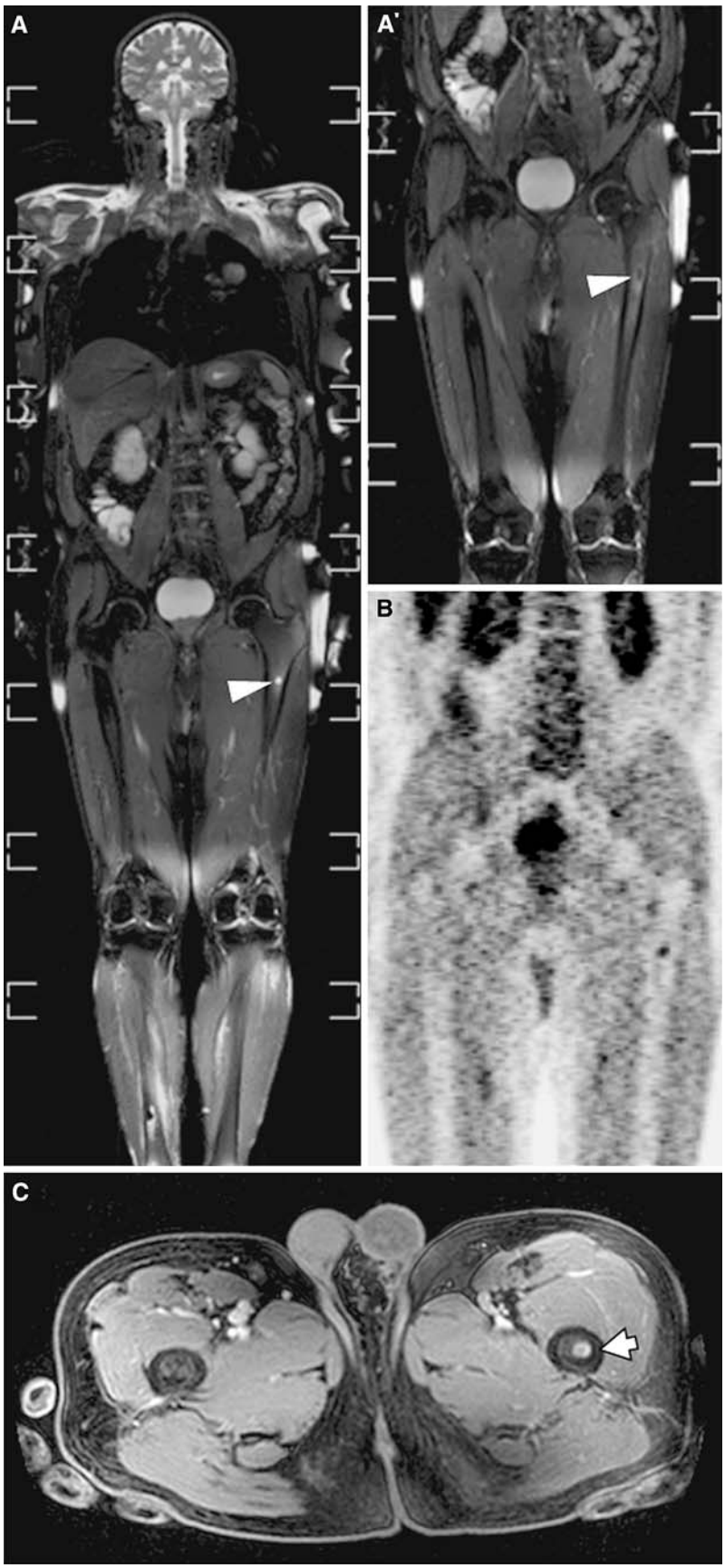

Fig. 8. Fifty-seven years-old patient with left femour metastasis. Coronal images T2W TSE STIR WB-MRI (**A**, **A'**), coronal PET image (**B**), axial T1W 3D FFE post-contrast image (**C**). Well defined hyperintense femour lesion on T2W TSE STIR images (*arrowheads*) demonstrates moderate metabolic uptake on PET image and significant contrast enhancement on T1W 3D FFE post-contrast image (*arrow*).

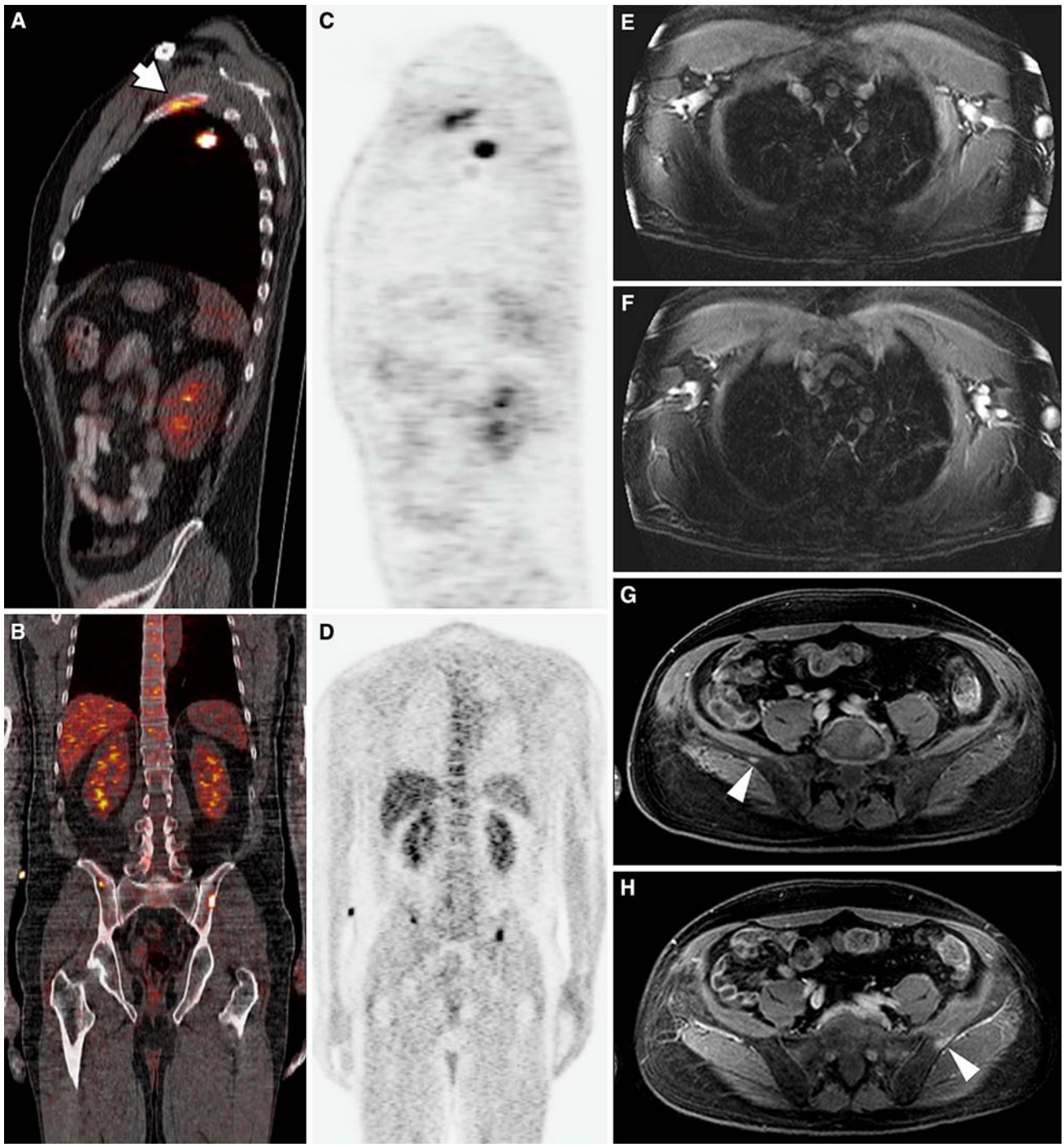

Fig. 9. Fifty-nine years-old patient with left rib and bilateral iliac bone metastasis. Sagittal (**A**) and coronal (**B**) PET-CT fused images and corresponding PET images (**C**, **D**), axial T1W 3D FFE post-contrast images (**E**–**H**). Bilateral iliac metastases are evident on both PET-CT and T1W FFE post-contrast images (*arrowheads*) while the small left rib lesion visible on PET-CT (*arrow*), was not detectable on corresponding MR images (**E**, **F**).

with some technical limitations. FDG is a nontumor-specific tracer and may accumulate at inflammatory foci with the risk of false positive findings and FDG concentration in the urinary tract may impair diagnostic performance.

While our study does not provide a statistical analysis of sensitivity, specificity and accuracy because of the low number of patients, WB-MRI, for its high contrast resolution, may represent a promising technique in CRC work-up, as an alternative to PET-CT with a trend of

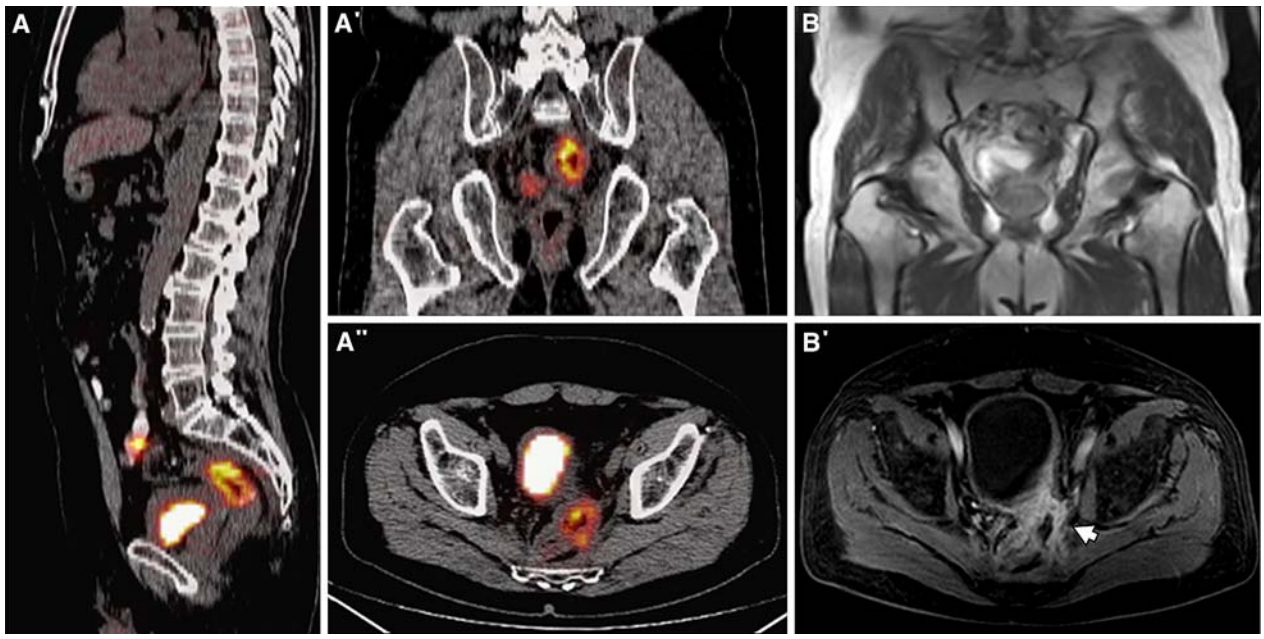

Fig. 10. Fifty-four years-old patient with local recurrence at surgery site. Sagittal, coronal and axial PET-CT fused images (**A**, **A′**, **A′**), coronal T2W TSE WB-MRI (**B**) and axial T1W 3D FFE post-contrast (**B′**). A high metabolic uptake lesion is visible on PET-CT with a tight correlation with c.e. WB-MRI (*arrow*).

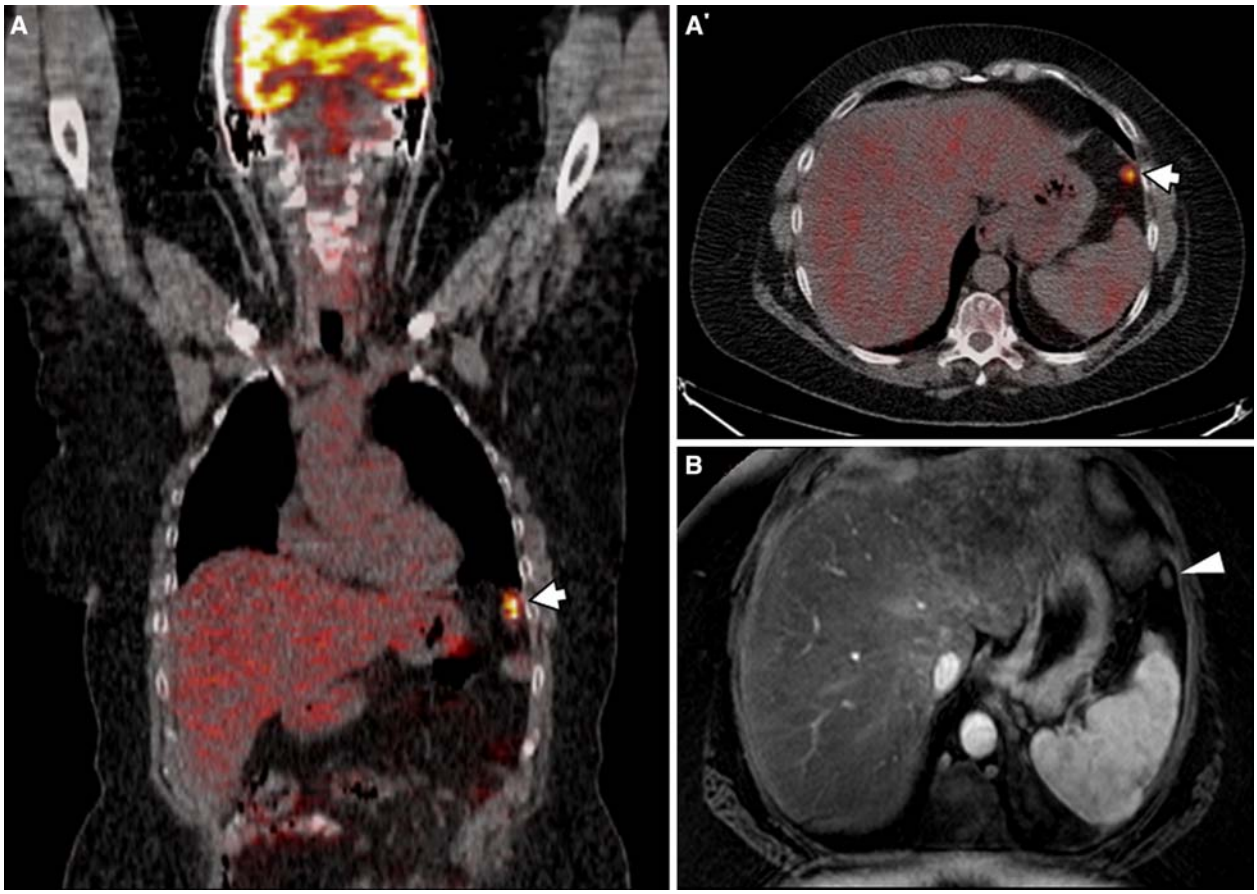

Fig. 11. Fifty-three years-old patient with metastatic peritoneal implant on the left anterior abdominal wall (*arrows*). Coronal and axial PET-CT fused images (**A**, **A′**) and axial T1W 3D FFE post-contrast (**B)** image. Metastatic implant with high metabolic activity on PET-CT images (*arrows* in (**A**,**A′**)) is also detected on the T1W 3D FFE post-contrast image (*arrowhead*).

superiority for brain and liver lesions. Larger clinical trials are necessary to provide long-term results and to determine the clinical impact of WB-MRI in CRC staging.

References

1. Ahmedin J, Rebecca S, Elizabeth W, et al. (2007) Cancer statistics, 2007. CA Cancer J Clin 57:43–66
2. Saunders TH, Mendes Ribeiro HK, Gleeson FV (2002) New techniques for imaging colorectal cancer: the use of MRI, PET and radioimmunoscintigraphy for primary staging and follow-up. Br Med Bull 64:81–99
3. Pickhardt P, Choi J, Hwang I, et al. (2003) Computed tomographic virtual colonoscopy to screen for colorectal neoplasia in asymptomatic adults. N Eng J Med 349:2191–2200
4. Lauenstein TC, Goehde SC, Herborn CU, et al. (2004) Whole-body MR imaging: evaluation of patients for metastases. Radiology 233:139–148
5. Schmidt GP, Baur-Melnyk A, Herzog P, et al. (2005) High-resolution whole-body magnetic resonance image tumor staging with the use of parallel imaging versus dual-modality positron emission tomography computed tomography: experience on a 32-channel system. Invest Radiol 40:743–753
6. Tausig A, Manthey N, Berger F, et al. (2000) Advantages and limitations of wholebody bone marrow MRI using Turbo-STIR sequences in comparison to planar bone scans. Nuklearmedizin 39:174–179
7. Eustace S, Tello R, DeCarvalho V, et al. (1997) A comparison of whole-body turboSTIR MR imaging and planar 99 mTc-methylene diphosphonate scintigraphy in the examination of patients with suspected skeletal metastases. AJR Am J Roentgenol 169:1655–1661
8. Iva K, Ludmila L, Otavar B, et al. (2003) Routine ^{18}F-FDG PET preoperative staging of colorectal cancer: comparison with conventional staging and its impact on treatment decision making. J Nucl Med 44(11):1784–1788
9. Dominique D , William HM (2004) PET and PET-CT evaluation of colorectal carcinoma. Semin Nucl Med 34(3):209–223
10. Abdel-Nabi H, Doerr RJ, Lamonica DM, et al. (1998) Staging of primary colorectal carcinomas with fluorine-18 fluorodeoxyglucose whole-body PET: correlation with histopathologic and CT findings. Radiology 206:755–760
11. Cohade C, Osman M, Leal J, et al. (2003) Direct comparison of (18)F-FDG PET and PET/CT in patients with colorectal carcinoma. J Nucl Med 44:1797–1803
12. Beyer T, Townsend DW, Brun T, et al. (2000) A combined PET/CT scanner for clinical oncology. J Nucl Med 4:1369–1379
13. Bar-Shalom R, Yefremov N, Guralnik L, et al. (2000) Clinical performance of PET/CT in evaluation of cancer: additional value for diagnostic imaging and patient management. J Nucl Med 44:1200–1209
14. Greene FL, Page DL, Fleming ID, et al. (eds). (2002) AJCC cancer staging manual, 6th edn. Springer, New York, NY
15. Flamen P, Stroobants S, Van Cutsem E (1999) Additional value of whole-body positron emission tomography with fluorine-18-2-fluoro-2- deoxy-d-glucose in recurrent colorectal cancer. J Clin Oncol 17:894–901
16. Lauenstein T, Freudenberg L, Goehde S, et al. (2002) Wholebody MRI using a rolling table platform for the detection of bone metastases. Eur Radiol 12:2091–2099
17. Horvath LJ, Burtness BA, McCarthy S, et al. (1999) Total-body echo-planar MR imaging in the staging of breast cancer: comparison with conventional methods-early experience. Radiology 211:119–128
18. Barkhausen J, Quick HH, Lauenstein T, et al. (2001) Whole body MR imaging in 30 seconds with real-time true FISP and a continuously rolling table platform: feasibility study. Radiology 220:252–256
19. Lauenstein TC, Goehde SC, Herborn CU, et al. (2002) Three-dimensional volumetric interpolated breath-hold MR imaging for whole-body tumor staging in less than 15 minutes: a feasibility study. AJR Am J Roentgenol 179:445–449
20. Pruessmann KP, Weiger M, Scheidegger MB, et al. (1999) SENSE: sensitivityencoding for fast MRI. Magn Reson Med 42:952–962
21. Eustace S, Walker R, Blake M, et al. (1999) Whole-body MR imaging. Practical issues, clinical applications, and future directions. Magn Reson Imaging Clin N Am 7:209–236
22. Antoch G, Vogt F, Freudenberg L, et al. (2003) Whole-body dualmodality PET/CT and whole-body MRI for tumor staging in oncology. JAMA 290:3199–3206
23. Muller-Horvat C, Radny P, Eigentler TK, et al. (2006) Prospective comparison of the impact on treatment decisions of whole-body magnetic resonance imaging and computed tomography in patients with metastatic malignant melanoma. Eur J Cancer 42(3):342–350
24. Schlemmer HP, Schafer J, Pfannenberg C, et al. (2005) Fast whole-body assessment of metastatic disease using a novel magnetic resonance imaging system: initial experiences. Invest Radiol l40:64–71
25. Juergen FS, Heinz-Peter WS (2006) Total-body MR-imaging in oncology. Eur Radiol 16:2000–2015
26. Takahara T, Imay Y, Yamashita T, et al. (2004) Diffusion weighted whole body imaging with background body signal suppression (DWIBS): technical improvement using free breathing, STIR and high resolution 3D display. Radiat Med 22:275–282
27. Petra M, Carsten K, Frank T, et al. (2007) Diffusion-weighted whole-body MR imaging with background body signal suppression: a feasibility study at 3.0 Tesla. Eur Radiol 17(12):3031–3037
28. Semelka RC, Worawattanakul S, Kelekis NL, et al. (1997) Liver lesion detection, characterization, and effect on patient management: comparison of single-phase spiral CT and current MR techniques. J Magn Reson Imaging 7(6):1040–1047
29. Yang M, Martin DR, Karabulut N, et al. (2003) Comparison of MR and PET imaging for the evaluation of liver metastases. J Magn Reson Imaging 17(3):343–349
30. Richard CS, Diego RM, Cem B, et al. (2001) Focal liver lesions: comparison of dual-phase CT and multisequence multiplanar MR imaging including dynamic gadolinium enhancement. J Magn Reson Imaging 13(3):397–401
31. Rappeport ED, Loft A, Berthelsen AK, et al. (2007) Contrast-enhanced FDG-PET/CT vs. SPIO-enhanced MRI vs. FDG-PET vs. CT in patients with liver metastases from colorectal cancer: a prospective study with intraoperative confirmation. Acta Radiol 48(4):369–378
32. Rappeport ED, Loft A (2007) Liver metastases from colorectal cancer: imaging with superparamagnetic iron oxide (SPIO)-enhanced MR imaging, computed tomography and positron emission tomography. Abdom Imaging 32(5):624–634
33. Steinborn (1999) Whole-body bone marrow MRI in patients with metastatic disease to the skeletal system. J Comput Assist Tomogr 23:123–129